Research Square

Preprints are preliminary reports that have not undergone peer review.
They should not be considered conclusive, used to inform clinical practice,
or referenced by the media as validated information.

Integrated Computational, Metabolomic, and Experimental Pharmacological Approaches for Anti-inflammatory Activity in Psychotria viridiflora Reinw. ex Blume

Retno Widyowati

rr-retno-w@ff.unair.ac.id

Universitas Airlangga

Irawati Sholikhah

Universitas Airlangga

Rizki Rahmadi Pratama

Islamic University of Kalimantan Muhammad

Qiara Amelia Putri Priyono

Universitas Airlangga

Dhea Anggraini

Universitas Airlangga

Azzalin Devariany Mufida

Universitas Airlangga

Sausan Syahira Arsyie

Universitas Airlangga

Meiza orchid dewani suhanto

Universitas Airlangga

Suciati Suciati

Universitas Airlangga

Yiwei Wang

Nanjing University of Chinese Medicine

Masayoshi Arai

The University of Osaka

Hsin-I Chang

National Chiayi University

Research Article

Keywords: Psychotria viridiflora, Osteoarthritis, RAW 264.7, Metabolomics, Molecular Docking

Posted Date: November 24th, 2026

DOI: https://doi.org/10.21203/rs.3.rs-10572310/v1

License: This work is licensed under a Creative Commons Attribution 4.0 International License.
Read Full License

Additional Declarations: No competing interests reported.

Integrated Computational, Metabolomic, and Experimental Pharmacological Approaches for Anti-inflammatory Activity in *Psychotria viridiflora* Reinw. ex Blume

Retno Widyowati[1,2,3*], Irawati Sholikhah[1], Rizki Rahmadi Pratama[4], Qiara Amelia Putri Priyono[5], Dhea Anggraini[5], Azzalin Devariany Mufida[5], Sausan Syahira Arsyie[5], Meiza Orchid Dewani Suhanto[5], Suciati Suciati[1,2,3], Yiwei Wang[6], Masayoshi Arai[7], Hsin-I Chang[8]

[1]Department of Pharmaceutical Sciences, Faculty of Pharmacy, Universitas Airlangga, Nanizar Zaman Joenoes Building, Campus C, Mulyorejo, Surabaya 60115, East Java, Indonesia
[2]Ethnomedicine and Indonesian Traditional Medicine Development Research Center, Faculty of Pharmacy, Universitas Airlangga, Mulyorejo, Surabaya, East Java 60115, Indonesia
[3]Skin and Cosmetic Technology (ICT) Center of Excellence, Universitas Airlangga, Mulyorejo, Surabaya, East Java 60115, Indonesia
[4]Department of Pharmaceutical Sciences, Faculty of Pharmacy, Islamic University of Kalimantan Muhammad Arsyad Al Banjari, Jl. Adhyaksa No. 2, Kayu Tangi, Banjarmasin 70123, South Kalimantan, Indonesia.
[5]Undergraduate student of Pharmaceutical Sciences, Faculty of Pharmacy, Universitas Airlangga, Nanizar Zaman Joenoes Building, Campus C, Mulyorejo Street, Surabaya 60115, East Java, Indonesia
[6]School of Pharmacy, Nanjing University of Chinese Medicine, No. 138 Xianlin Avenue, Qixia District, Nanjing, Jiangsu 210023, People's Republic of China
[7] Laboratory of Natural Products for Drug Discovery, Graduate School of Pharmaceutical Sciences, The University of Osaka, 1-6 Yamadaoka, Suita, Osaka 565-0871, Japan.
[8] Department of Biochemical Science and Technology, College of Life Sciences, National Chiayi University, No. 300 Syuefu Road, East District, Chiayi City 600355, Taiwan (R.O.C.).

*Corresponding author: Retno Widyowati
Department of Pharmaceutical Sciences, Faculty of Pharmacy, Nanizar Zaman Joenoes Building, Campus C, Universitas Airlangga, Mulyorejo Street, Surabaya 60115, East Java, Indonesia, +6281615886978

ABSTRACT

Osteoarthritis (OA), a prevalent degenerative joint disease characterized by inflammation and dysregulation of nitric oxide (NO) and interleukin-1β (IL-1β), has traditionally been managed with *Psychotria viridiflora*. This study aimed to scientifically validate its anti-OA potential through integrated computational, metabolomic, and experimental approaches. LC-HRMS analysis of the 70% ethanol extract identified 39 compounds, prominently phenolics and flavonoids (e.g., isorhamnetin, quercetin, scutellarin, rutin), and alkaloids (berberine). Molecular docking against Type-1 Interleukin-1 Receptor (1ITB) and human INOSOX (3E7G) revealed strong binding affinities for several identified compounds, with flavonoids consistently showing high affinity for both targets. In vitro, the extract significantly suppressed NO production in LPS-stimulated RAW 264.7 cells at 15 and 25 μg/mL, maintaining over 90% cell viability. In vivo studies in MIA-induced OA rats demonstrated significant therapeutic effects after 28 days of treatment. Administering the extract at 5, 10, and 20 mg/200 g BW significantly extended pain latency in a dose-dependent manner and reduced joint diameter ($p < 0.05$ in both cases). Furthermore, the extract significantly lowered serum IL-1β levels, with reductions ranging from 761.33 to 594.67 pg/mL across the tested doses, compared with the negative control (1957.33 pg/mL). These findings collectively indicate that *P. viridiflora* extract has promising anti-OA properties, mediated by its diverse

bioactive compounds and their interactions with key inflammatory targets, providing a scientific basis for its traditional use.

Keywords: *Psychotria viridiflora,* Osteoarthritis, RAW 264.7, Metabolomics, Molecular Docking

INTRODUCTION

One frequently occurring degenerative illness with slow progression is osteoarthritis (OA). Articular cartilage typically deteriorates in OA for pathologic, physiological, metabolic, and biochemical reasons. According to Arden et al. (2018), osteophytes (growths at the ends of joints) cause inflammation and joint degeneration in the connecting muscles, while damage to the joint's hyaline cartilage, thickening of the subchondral bone, and ossification of the bony plates are also characteristics of the condition (Arden et al., 2018). Age, gender, heredity, obesity, and joint injuries (especially those sports-related) are among the frequent risk factors that lead to its occurrence (Heijink et al., 2012).

In OA, various joint tissues, such as chondrocytes (cartilage cells) and synoviocytes (joint lining cells), produce more inflammatory cytokines in response to biomechanical disruptions and inflammatory signals (Goldring & Otero, 2011). Chondrocytes, the main type of cartilage cell, are central to OA pathophysiology because they produce interleukin-1β (IL-1β) and tumor necrosis factor-alpha (TNF-α) in response to inflammatory stimuli and mechanical stress. These cytokines are strong inflammatory mediators that also induce cartilage deterioration (Leong et al., 2013; Rajapakse et al., 2018).

Matrix metalloproteinases (MMPs), whose synthesis is stimulated by TNF-α and IL-1β, are enzymes that degrade cartilage's extracellular matrix (Henao-Murillo et al., 2021). Collagen and proteoglycans, two cartilage matrix components destroyed by MMPs and implicated in OA development, are major targets. Moreover, IL-1 and TNF-α increase cyclooxygenase-2 (COX-2) activity (Henao-Murillo et al., 2021), which produces prostaglandin E2 (PGE2), a potent inflammatory mediator (Eitner et al., 2021). Increased PGE2 production further contributes to inflammation and pain within the joint. This cascade of events involving IL-1, TNF-α, COX-2, MMPs, and PGE2 illustrates the complex inflammatory processes underlying OA and highlights potential targets for therapeutic interventions aimed at reducing inflammation and hindering disease progression (Leonidou et al., 2018).

Degeneration of the underlying bone and joint cartilage characterizes OA, a prevalent form of arthritis (Leong et al., 2013). IL-1β and nitric oxide (NO) play substantial roles in the inflammatory response associated with OA. Various cells, including synovial cells, macrophages, and chondrocytes (the cells that make up cartilage), secrete the pro-inflammatory cytokine IL-1β (Eitner et al., 2021). It stimulates the production of other inflammatory mediators and enzymes, including MMPs and disintegrin and metalloproteinases with thrombospondin motifs (ADAMTSs) (Leonidou et al., 2018). These enzymes contribute to cartilage breakdown in OA by degrading extracellular matrix components (Smith & Baird, 2023). NO is a signaling molecule involved in various physiological processes. In OA, the NO produced by chondrocytes and synovial cells in response to inflammatory stimuli induces the expression of MMPs and ADAMTSs in chondrocytes, further contributing to cartilage degradation.

One of the most frequent symptoms of OA, prompting those affected to seek medical attention, is pain. In the management of OA-induced pain and inflammation, the administration of nonsteroidal anti-inflammatory medications (NSAIDs) is a frequently recommended pharmacological therapy. On the other hand, long-term NSAID use is associated with several negative side effects such as inhibited kidney function, cardiovascular problems, and gastrointestinal conditions (for example, ulcers and bleeding) (Kolasinski et al., 2019).

Psychotria viridiflora Reinw. Ex Blume, a plant species in the *Psychotria* genus, belongs to the Rubiaceae family. Native to parts of Southeast Asia, including Indonesia and Malaysia, *P. viridiflora* is used in traditional medicine for its purported analgesic (pain-relieving) and anti-inflammatory properties. However, research on the pharmacological properties and bioactive compounds of *P. viridiflora* is relatively limited compared to that on other plants (Solomon et al., 2011).

Formagio et al. (2019) suggested that the administration of a 30 mg/kg BW dose of *P. colorata* to mice proved effective as an anti-inflammatory (Formagio et al., 2019). Furthermore, Yang et al. (2016) and Matsuura et al. (2013) indicated that *P. colorata* leaves and flowers contain alkaloids, particularly psychotridine, which exhibit strong analgesic properties. Moreover, *P. sarmentosa* Blume leaves have substantial analgesic and anti-inflammatory properties that may alleviate arthritis-related symptoms (Yang et al., 2016; Matsuura et al., 2013). The decision to evaluate the in vivo anti-inflammatory potential of *P. viridiflora* is strongly grounded in previous experimental evidence demonstrated across the genus *Psychotria*. Phytochemical investigations of closely related species, such as *P. stenocalyx* and *P. leiocarpa*, confirmed that indole alkaloids (e.g., vincosamide) and flavonoid constituents significantly suppress chemically induced inflammation, leukocyte migration, and edema formation in rodent models (Queiroz et al., 2017; Formagio et al., 2019). Furthermore, in vivo evaluations of *P. malayana* extracts demonstrated a modulating effect on the inflammatory and proliferative phases of tissue injury, promoting angiogenesis and fibroblast synthesis in rats (Fairuz et al., 2023).

Although computational and in vitro screenings provide preliminary evidence of enzymatic binding (e.g., COX-2 and cytokine inhibition), in vitro assay systems cannot reflect complex systemic pharmacokinetics, vascular permeability changes, or organ-level tissue responses. Therefore, given the established in vivo anti-inflammatory efficacy of bioactive indole alkaloids and flavonoids reported in *P. congeners*, an in vivo animal study of *P. viridiflora* is scientifically essential to validate its systemic therapeutic efficacy and physiological mechanism of action.

Furthermore, recent pharmacological evaluations of plant-derived secondary metabolites targeting NO production and inducible nitric oxide synthase (iNOS) pathway modulation strongly support investigating anti-inflammatory mechanisms in joint-related pathologies (Sari et al., 2023; Widyowati et al., 2021; Khotib et al., 2020). Overproduction of NO by chondrocytes significantly accelerates cartilage degradation, extracellular matrix destruction, and joint discomfort in osteoarthritis (Sari et al., 2023). While computational molecular docking and in vitro macrophage assays provide foundational insights into anti-inflammatory target interactions, establishing therapeutic bioavailability, tissue-level protection,

and dose-dependent efficacy requires comprehensive in vivo pharmacological validation using standardized joint inflammation models.

This study investigated key components of the OA pain response, including NO and IL-1β production. The research was divided into two experimental categories: an in vitro test of lipopolysaccharide (LPS)-induced NO inhibition using RAW 264.7 cells and an in vivo test of anti-OA characteristics in rats subjected to monosodium iodoacetate (MIA) induction.

MATERIALS AND METHODS

Materials

Aqueous and ethanol p.a. (Merck, Jakarta, INA) were used for the extraction process. In vitro assays utilized Dulbecco's modified Eagle's medium (DMEM), fetal bovine serum (FBS), dimethyl sulfoxide (DMSO) (Sigma-Aldrich, Darmstadt, Germany), amphotericin B, streptomycin, penicillin (all obtained from Thermo Fisher Scientific, Jakarta, INA), 2,5-diphenyltetrazolium bromide (MTT), sodium nitrite, lipopolysaccharide (LPS), and Griess reagent. In vivo assays employed sodium carboxymethyl cellulose (CMC-Na), 0.9% physiological saline, 10% ketamine (Agro-veterinarian, Nicaragua), 1% xylazine, MIA (Sigma-Aldrich, Surabaya, INA), meloxicam 7.5 mg (Sanbe Farma, Indonesia), and an IL-Iβ ELISA kit (Bioenzy, Germany). *P. viridiflora* was sourced from East Kotawaringin Regency, Central Kalimantan, Indonesia.

Untargeted metabolomics analysis was conducted using a Thermo Scientific™ Vanquish™ Horizon UHPLC system with an Accucore™ Phenyl Hexyl column, coupled with a Thermo Scientific™ Orbitrap™ Exploris 240 HRMS featuring an Optamax™ NG Heated ESI source. Sample preparation involved vortex homogenization and 0.20 µm nylon filtration, with mobile phases comprising MS-grade water and acetonitrile (both with 0.1% formic acid). Data processing and compound identification were performed using Thermo Scientific™ Compound Discoverer 3.3, referencing the mzCloud Library, ChemSpider Database, and various mass list databases. For in silico investigations, protein targets included human INOSOX (PDB ID: 3E7G) and Type-1 Interleukin-1 Receptor (PDB ID: 1ITB), both 2.50 Å X-ray crystallographic structures from Homo sapiens expressed in Escherichia coli retrieved from the Protein Data Bank (www.rcsb.org).

Plant Material Collection and Identification

Fresh leaves of *P. viridiflora* were collected from private agricultural land located in East Kotawaringin Regency, Central Kalimantan, Indonesia. Sampling was conducted with the private landowner's explicit permission. The collected species are wild-harvested, non-endangered, and not subject to restricted conservation regulations. Dr. Silva Abraham, S.Si., M.Si., a plant taxonomist at the Herbarium Bogoriense, National Research and Innovation Agency (BRIN), Bogor, Indonesia, conducted formal botanical identification and authentication. A representative voucher specimen (Voucher Specimen No. B-3971/II.6.2/DI.05.07/10/2022) has been deposited in the institutional herbarium for future reference. The "Herbarium Bogoriense" leaves were chopped, divided into small piles, and dried

before being blended into a 1000-gram dried powder. 5000 cc of 70% ethanol (1:5) was used for a 24-hour maceration to extract the dried plant, which was subsequently macerated twice more. Using a rotary evaporator set at 40°C and 40 rpm, the filtrate was evaporated to produce a thick extract of consistent weight.

Metabolomics Using LC-HRMS

Untargeted metabolomic analysis was conducted at the Corpora Science Research Laboratory in Yogyakarta, Indonesia, using dual-mode electrospray ionization (ESI+, ESI-). Chromatographic separation was performed on a Thermo Scientific™ Vanquish™ Horizon UHPLC system utilizing a Thermo Scientific™ Accucore™ Phenyl Hexyl column (100 mm × 2.1 mm, 2.6 µm) at 40 °C. The mobile phase comprised MS-grade water with 0.1% formic acid (A) and acetonitrile with 0.1% formic acid (B), delivered at 0.3 mL/min over a 15-minute gradient (5-98% B). A 5 µL sample was injected. High-resolution mass spectrometry was carried out using a Thermo Scientific™ Orbitrap™ Exploris 240 HRMS, acquiring data in Full MS/dd-MS2 mode with polarity switching.

Full MS resolution was 60,000 FWHM (67-1000 m/z), and dd-MS2 resolution was 15,000 FWHM with NCEs of 30, 50, and 150. Ionization was achieved via an Optamax™ NG Heated Electrospray Ionization (H-ESI) source (positive: 3800 V; negative: 2500 V), with sheath, auxiliary, and sweep gas flows of 40, 8, and 1 AU, respectively, and ion transfer tube/vaporizer temperatures of 300°C and 250°C, respectively. Samples were prepared by vortex homogenization and 0.20 µm filtration before injection. Data processing and compound identification were performed using Thermo Scientific Compound Discoverer 3.3, referencing the mzCloud Library, ChemSpider Database, and various mass list databases (e.g., Arita Lab Flavonoid, Endogenous Metabolites, Natural Products Atlas).

Molecular Docking

The in silico investigation utilized two protein targets: human INOSOX (PDB ID: 3E7G) and Type-1 Interleukin-1 Receptor (PDB ID: 1ITB), both X-ray crystallographic structures (2.50 Å resolution) from Homo sapiens and retrieved from the Protein Data Bank (www.rcsb.org). Ligands, identified from LC-MS/MS data, were obtained from PubChem, prepared with Marvin Sketch 20.21, and energy-minimized using the MMFF94 force field. Protein preparation involved removing water molecules, adding missing residues and hydrogen atoms, and energy minimization using the GROMOS96 force field. A semi-flexible docking method was applied, with grid boxes (0.375 Å point distance) centered appropriately for each protein (1ITB: 60x60x60 pixels at x=48.729, y=3.25, z=16.546; 3E7G: 40x40x40 pixels at x=55.232, y=21.838, z=78.677). Molecular docking was executed using the Lamarckian Genetic Algorithm (population size 150, 2,500,000 evaluations, 100 runs). Optimal poses were determined based on the lowest binding energy (G), inhibition constant (Ki), and essential amino acid interactions, visualized in Discovery Studio Visualizer.

Cell culture

The RAW 264.7 cell line, supplied by the Department of Biochemical Science and Technology, National Chiayi University, Taiwan, was cultivated in DMEM supplemented with 10% FBS and 1%

penicillin-streptomycin liquid. The culture was maintained in an incubator at 37°C, 5% CO_2, and 95% humidity (Yan et al., 2017; Widyowati et al., 2021).

MTT assay

Viability of the RAW 264.7 cell line was assessed using a 100 µL final-volume MTT colorimetric assay (Sigma-Aldrich). The cell lines were plated in a 96-well plate with 2×10^4 cells per well. After a 24-hour incubation period, the cells were subjected to successive doses of 70% ethanol extract of *P. viridiflora* for a further 24 hours. 100 µL of MTT was subsequently added to the medium, which was incubated for five hours. To dissolve the formazan, 100 µL of DMSO was added after the supernatants had been removed. After gentle agitation of the plate, absorbance at 570 nm was measured using a microplate reader (Yan et al., 2017; Widyowati et al., 2021).

NO production assay

RAW 264.7 cells were cultivated on a 24-well plate at a density of 2×10^5 cells per well. After a 24-hour incubation, the cells were treated with 1 g/ml LPS. Griess reagent was used to determine whether nitrite was present in a 100 µL culture medium sample. The absorbance at 550 nm was then measured using an ELISA reader (Widyowati et al., 2021; Nagy et al., 2021).

Animals and ethical approval

All animal procedures were approved by the Animal Ethics Committee of the Faculty of Veterinary Medicine, Universitas Airlangga, Surabaya, Indonesia (Ethical Clearance No. 2.KEH.118.07.2025) and were performed in accordance with relevant guidelines and regulations. The study is reported in accordance with the ARRIVE 2.0 guidelines; the completed ARRIVE Essential 10 checklist is provided as Additional file 1. The experimental unit was the individual animal.

Thirty healthy male Wistar rats (*Rattus norvegicus*; outbred, not genetically modified), aged 2–4 months, were purchased from Pusat Veteriner Farma (PUSVETMA), Surabaya, Indonesia; group mean body weights at baseline ranged from 169.6 to 184.2 g. The rats were housed five per cage on wood-shaving bedding, which was changed every 2–3 days, in the Animal Laboratory of the Faculty of Pharmacy, Universitas Airlangga, under a 12 h light/dark cycle at 22–24 °C and 50–60% relative humidity, with standard pellet feed and clean drinking water available *ad libitum*. All animals were acclimatized for 7 days before the experiment. Inclusion criteria were clean fur, bright eyes, active locomotion, absence of physical defects, and successful completion of acclimatization. Animals showing >10% body-weight loss during acclimatization, physical abnormalities, or signs of joint inflammation at baseline were excluded before group allocation.

The sample size was calculated with the formula of Charan and Kantharia (2013), $n = 2SD^2(Z_{\alpha/2} + Z_{\beta})^2/d^2$, using hot-plate latency values reported by Khotib *et al.* (2020): the expected effect size (d = 5.34 s) was the increase in latency from day 21 to day 49 in the meloxicam–glucosamine 250 mg group (16.93 to 22.27 s), and the standard deviation (SD = 2.85 s) was that of the glucosamine 500 mg group on day 49; α was set at 0.05 ($Z_{\alpha/2} = 1.96$) and power at 80% ($Z_{\beta} = 0.842$). The calculation yielded n = 4.47, so

five rats per group were used, for a total of 30 rats in six groups. Hot-plate latency, the outcome used for this calculation, was therefore the primary outcome.

Each rat was given a unique identification code. Allocation to the six groups was performed by stratified block randomization based on body weight: the rats were ranked by body weight and divided into five blocks of six, and the six rats within each block were randomly assigned, one to each group, using a computer-generated sequence (www.randomizer.org). Cages and samples were labeled only with codes, and the investigators who performed the hot-plate test, knee-diameter measurements, and IL-1β ELISA were blinded to group allocation.

Humane endpoints defined in the approved protocol were body-weight loss >20%, refusal of food or water for >24 h, severe ulceration at the injection site, or a moribund state (extreme lethargy); any animal reaching one of these endpoints was to be euthanized immediately. No animal reached a humane endpoint or died during the study, and all 30 animals (n = 5 per group) were included in every analysis.

On day 49, after the final hot-plate and knee-diameter measurements, the rats were deeply anesthetized with ketamine (80 mg/kg BW) and xylazine (10 mg/kg BW) administered intraperitoneally, and the final tail-vein blood sample was collected (see IL-1β cytokine assay). After loss of consciousness and loss of the pedal withdrawal reflex had been confirmed, the rats were exsanguinated by cardiac puncture, and death was ensured by thoracotomy.

Rat model

Rats were split into six groups: the healthy control group received unlimited food and drink, 0.5% CMC-Na for the negative group, 0.135 mg/200 g BW of meloxicam for the positive group, and doses of 5, 10, and 20 mg/200 g BW of a 70% ethanol extract of *P. viridiflora* leaves for the three treatment groups (Nagy *et al*., 2017; Widyowati *et al*., 2019; Widyowati *et al*., 2023). OA was induced on day 1, after baseline measurements on day 0. Rats in all groups except the healthy control group were anesthetized with ketamine (80 mg/kg BW) and xylazine (5 mg/kg BW) intraperitoneally and received a single intra-articular injection of MIA (4 mg in 50 µL of 0.9% saline, sterilized through a 0.22 µm filter) into the right knee through the infrapatellar ligament, with the knee flexed at 90°, using a 30G needle. The healthy control group received neither MIA nor treatment. From day 21 to day 48 (28 days), the vehicle, meloxicam, or extract, each suspended in 0.5% CMC-Na (1 mL/200 g BW), was administered once daily by oral gavage.

Hyperalgesia experiment

On days 0, 7, 14, 21, 28, 35, 42, and 49, a hot plate was used as a nociceptive heat stimulus to evaluate pain in all groups. The range of possible hyperalgesia responses, including jumping, foot stamping, or licking the rear paw, was recorded as soon as the rats were placed on the heated surface. For the test, rats were placed individually on a hot plate set to 55°C (Nagy et al., 2017; Widyowati et al., 2019; Widyowati et al., 2023; Sari et al., 2023).

Joint swelling measurement

The method described above was used to determine whether joint tissue enlargement, a sign of synovial inflammation in OA, was present. On days 0, 7, 14, 21, 28, 35, 42, and 49, the right knee of each rat (ipsilateral) was measured with a calibrated vernier caliper (Nagy et al., 2017; Widyowati et al., 2019; Widyowati et al., 2023; Sari et al., 2023).

IL-1β cytokine assay

Blood samples were extracted from the tail vein and transferred to a blood collection container on days 21 and 49. A centrifuge set at 3000 rpm was used to extract blood serum. In accordance with the manufacturer's instructions, commercial rat IL-1β ELISA kits (Bioenzy) were used to measure the levels of IL-1β. The results were analyzed using an ELISA Reader Instrument. Before blood extraction via the tail vein, the rats were anesthetized with a combination of ketamine (80 mg/kg BW) and xylazine (10 mg/kg BW) injected intraperitoneally to minimize stress and unwanted movement. After the rats showed no response to pain stimuli, blood sampling was performed. On completion of the final blood sampling, the animals were euthanized as described in the Animals and ethical approval section (Widyowati *et al*., 2023; Sari *et al*., 2023).

Statistical analysis

Rat experimental data were presented as the mean ± SD of five rats in each group. The individual rat was the unit of analysis. Before parametric testing, normality was assessed with the Shapiro–Wilk test (knee diameter and IL-1β) or the Kolmogorov–Smirnov test (hot-plate latency), and homogeneity of variance with Levene's test; all datasets met these assumptions ($p > 0.05$). All statistical analyses were performed using one-way and two-way ANOVA in SPSS with 95% confidence intervals ($p<0.05$). Then, post hoc tests for least significant difference were run to identify significant differences between groups. In addition, IL-1β levels before and after treatment were compared within each group using a paired t-test, and the healthy and MIA-induced groups before treatment were compared using an independent-samples t-test.

RESULTS AND DISCUSSION

Metabolomic Analysis

Table 1 Metabolomic Analysis Based On LC-HRMS Results

No.	Name	Formula	Calc. MW	m/z	RT [min]
1	Choline	$C_5H_{13}NO$	103.0996	104.1069	0.696
2	D-(-)-Quinic acid	$C_7H_{12}O_6$	192.0631	191.0558	0.701
3	Betaine	$C_5H_{11}NO_2$	117.0787	118.0860	0.710
4	Proline	$C_5H_9NO_2$	115.0631	116.0704	0.713
5	Gluconic acid	$C_6H_{12}O_7$	196.0580	195.0507	0.737
6	D-(+)-Malic acid	$C_4H_6O_5$	134.0213	133.0141	0.817
7	Succinic acid	$C_4H_6O_4$	118.0264	117.0191	1.029
8	3-Hydroxybutyric acid	$C_4H_8O_3$	104.0472	103.0399	1.135
9	2.3-Dihydroxybenzoic acid	$C_7H_6O_4$	154.0264	153.0191	1.142

10	Gallic acid	$C_7H_6O_5$	170.0213	169.0140	1.147
11	Levulinic acid	$C_5H_8O_3$	116.0471	115.0399	1.437
12	Methylsuccinic acid	$C_5H_8O_4$	132.0421	131.0348	1.522
13	3.4-Dihydroxyphenylacetic acid	$C_8H_8O_4$	168.0421	167.0348	1.553
14	Apocynin	$C_9H_{10}O_3$	166.0628	167.0701	1.617
15	3.5-Dihydroxybenzoic acid	$C_7H_6O_4$	154.0264	153.0191	1.821
16	Catechol	$C_6H_6O_2$	110.0366	109.0293	1.837
17	trans-3-Indoleacrylic acid	$C_{11}H_9NO_2$	187.0631	188.0703	1.906
18	2.5-Dihydroxybenzaldehyde	$C_7H_6O_3$	138.0315	137.0242	2.247
19	8-Hydroxyquinoline	C_9H_7NO	145.0526	146.0599	2.402
20	Salicylic acid	$C_7H_6O_3$	138.0315	137.0242	2.484
21	Chlorogenic acid	$C_{16}H_{18}O_9$	354.0942	353.0866	2.524
22	4-Anisic acid	$C_8H_8O_3$	152.0472	151.0399	2.683
23	Hexanoic acid	$C_6H_{12}O_2$	116.0835	115.0763	3.315
24	Scutellarin	$C_{21}H_{18}O_{12}$	462.0789	463.0863	3.360
25	Vanillic acid	$C_8H_8O_4$	168.0420	167.0348	3.635
26	L-Phenylalanine	$C_9H_{11}NO_2$	165.0787	164.0715	3.671
27	Rutin	$C_{27}H_{30}O_{16}$	610.1525	611.1597	3.704
28	Quercetin	$C_{15}H_{10}O_7$	302.0422	303.0495	4.259
29	Genistin	$C_{21}H_{20}O_{10}$	432.1049	433.1122	4.556
30	Pelargonidin	$C_{15}H_0O_5$	270.0519	271.0592	4.602
31	Berberine	$C_{20}H_{17}NO_4$	335.1155	336.1228	5.357
32	Fisetin	$C_{15}H_{10}O_6$	286.0474	287.0546	5.683
33	Isorhamnetin	$C_{16}H_{12}O_7$	316.0580	317.0653	5.779
34	Luteolin	$C_{15}H_{10}O_6$	286.0474	285.0401	6.497
35	Isoliquiritigenin	$C_{15}H_{12}O_4$	256.0732	257.0804	7.182
36	(+/-)12(13)-DiHOME	$C_{18}H_{34}O_4$	314.2455	313.2381	8.890
37	(+/-)9,10-dihydroxy-12Z-octadecenoic acid	$C_{18}H_{34}O_4$	314.2452	313.2380	9.141
38	(±)9-HpODE	$C_{18}H_{32}O_4$	312.2296	311.2224	9.218
39	Oleoyl ethanolamide	$C_{20}H_{39}NO_2$	325.2976	326.3049	10.023

The untargeted metabolomic analysis of the extract revealed a diverse phytochemical profile, encompassing 39 distinct compounds. Significantly, the identified metabolites included a rich array of phenolic compounds and flavonoids such as salicylic acid, chlorogenic acid, gallic acid, rutin, genistin, fisetin, quercetin, scutellarin, luteolin, and isorhamnetin. These classes of compounds are widely recognized for their potent antioxidant and anti-inflammatory properties, suggesting a significant contribution to the extract's potential therapeutic effects. Furthermore, the presence of alkaloids such as berberine, various organic acids (e.g., gluconic acid, succinic acid), and fatty acid derivatives (e.g., oleoyl ethanolamide, dihydroxy-octadecenoic acids) indicates a broad spectrum of bioactive constituents, as shown in Table 1.

Each identified metabolite was characterized by its specific retention time and mass-to-charge ratio, facilitating a comprehensive understanding of the chemical diversity inherent in the extract (Zhu et al., 2023). To further validate these findings, untargeted metabolomic data were integrated with MS2

fragmentation patterns and cross-referenced with established databases to ensure the accurate classification of primary metabolites in both positive and negative ionization modes (Dogan, 2024). Beyond these primary metabolites, qualitative screenings further indicated the presence of terpenoids, tannins, and reducing sugars within the aqueous matrix, while saponins were notably absent (Chen et al., 2021).

The presence of these identified compounds (e.g., chlorogenic acid, rutin, quercetin, berberine, gallic acid, and others) in *P. viridiflora* or other Rubiaceae plants could not be confirmed from the currently available sources, as no relevant data were found upon review. Rubiaceae species, including *Psychotria*, are generally rich in alkaloids, flavonoids, and phenolic acids. However, specific metabolomic studies linking the exact 39 compounds listed to *P. viridiflora* or close relatives are lacking here. Enabling web search or library access for academic databases is recommended to retrieve targeted phytochemical profiles and enable a detailed discussion. In addition to these specific identifications, the use of specialized software such as Compound Discoverer allows for the putatively assigned metabolites to be analyzed through fragmentation patterns, identifying complex structures such as polyols and various flavonoid derivatives that are typical secondary metabolic products in plant species (Berger et al., 2016; Kachlicki et al., 2016).

Molecular Docking Result

Molecular docking simulations against the Type-1 Interleukin-1 Receptor (PDB ID: 1ITB) revealed a range of binding affinities across the tested compounds, with binding energies from -8.14 kcal/mol to -1.66 kcal/mol and corresponding inhibition constants from 1.07 μM to 60.60 mM. Meloxicam showed the highest binding affinity, with a binding energy of -8.14 kcal/mol and an inhibition constant of 1.07 μM, suggesting strong potential as an IL-1β signaling inhibitor. Berberine, chlorogenic acid, and scutellarin also displayed strong affinities with binding energies of -7.55 kcal/mol (2.94 μM), -7.48 kcal/mol (3.31 μM), and -7.47 kcal/mol (3.37 μM), respectively. Other flavonoids such as genistin, isoliquiritigenin, fisetin, luteolin, rutin, quercetin, pelargonidin, and isorhamnetin consistently showed favorable binding energies below -6.0 kcal/mol, indicating their considerable inhibitory potential against this pro-inflammatory receptor, as shown in Table 2.

Direct docking data for chlorogenic acid and scutellarin in relation to IL-1β or related receptors were unavailable in the reviewed sources. The reviewed sources did not identify experimental in vitro or in vivo studies evaluating berberine, chlorogenic acid, and scutellarin in osteoarthritis models targeting IL-1β signaling or related pathways; therefore, a web or library search is recommended to obtain comprehensive validation data. Moreover, other flavonoids such as genistin, isoliquiritigenin, fisetin, luteolin, rutin, quercetin, pelargonidin, and isorhamnetin consistently showed favorable binding energies below -6.0 kcal/mol, indicating their considerable inhibitory potential against this pro-inflammatory receptor (Liu et al., 2023).

342 **Table 2** Molecular Docking Results PDB ID (1ITB)

No	Compound	Energy Binding (kcal/mol)	Inhibition Constant (μM)
1	Meloxicam	-8.14	1.07
2	Berberine	-7.55	2.94
3	Chlorogenic acid	-7.48	3.31
4	Scutellarin	-7.47	3.37
5	Genistin	-7.34	4.17
6	Isoliquiritigenin	-7.22	5.07
7	Fisetin	-7.18	5.50
8	Luteolin	-7.07	6.59
9	Rutin	-6.89	8.83
10	Quercetin	-6.84	9.70
11	Pelargonidin	-6.57	15.40
12	Isorhamnetin	-6.45	18.85
13	L-Phenylalanine	-5.92	45.72
14	Oleoyl ethanolamide	-5.72	63.77
15	(±)9-HpODE	-5.62	76.31
16	trans-3-Indoleacrylic acid	-5.41	108.10
17	Apocynin	-5.06	196.87
18	(+/-)12(13)-DiHOME	-5.02	209.57
19	8-Hydroxyquinoline	-4.87	271.13
20	(+/-)9,10-dihydroxy-12Z-octadecenoic acid	-4.69	365.69
21	3.4-Dihydroxyphenylacetic acid	-4.64	397.44
22	Vanillic acid	-4.39	601.98
23	2.5-Dihydroxybenzaldehyde	-4.26	748.34
24	Proline	-4.23	797.40
25	D-(-)-Quinic acid	-4.21	818.24
26	2.3-Dihydroxybenzoic acid	-4.19	849.13
27	3.5-Dihydroxybenzoic acid	-4.06	1600
28	Gallic acid	-4.03	1110
29	4-Anisic acid	-4.03	1110
30	Catechol	-3.81	1620
31	Salicylic acid	-3.78	1690
32	Hexanoic acid	-3.52	2620
33	Gluconic acid	-3.47	2840
34	Choline	-3.29	3850
35	Levulinic acid	-2.93	7120
36	Betaine	-2.86	8040
37	3-Hydroxybutyric acid	-2.80	8890
38	Methylsuccinic acid	-2.14	27080
39	Succinic acid	-1.74	52590
40	D-(+)-Malic acid	-1.66	60600

343

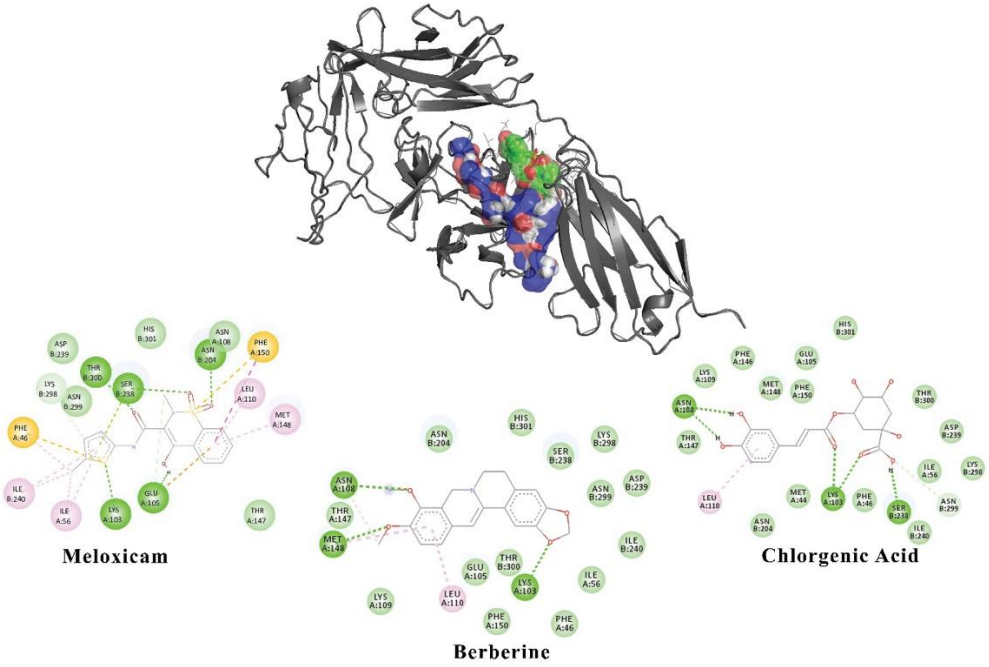

Figure 1. 3D Visualization of top three compounds - PDB ID 1ITB

Figure 1 presents a three-dimensional visualization of the 1ITB protein structure in a gray ribbon model. In the active site of the Interleukin-1 Type-1 receptor, the three compounds with the highest binding affinity - Meloxicam, Berberine, and Chlorogenic Acid - occupy the same position, indicating potential competition for a similar binding pocket. In addition, a two-dimensional interaction diagram details the specific chemical bonds of each compound: Meloxicam forms an extensive interaction network that includes hydrogen and hydrophobic bonds with residues GLU A:105 and LYS A:103; Berberine interacts with ASN A:108 and MET A:148; and Chlorogenic Acid interacts with ASN A:108 and THR A:147.

For the human INOSOX protein (PDB ID: 3E7G), the molecular docking results indicated even stronger binding affinities for several compounds, with binding energies ranging from -8.13 kcal/mol to -3.00 kcal/mol and inhibition constants from 1.09 μM to 6.32 mM. Isorhamnetin was the most potent binder, with a binding energy of -8.13 kcal/mol and an inhibition constant of 1.09 μM. Scutellarin (-8.06 kcal/mol, 1.24 μM) and quercetin (-7.96 kcal/mol, 1.47 μM) also showed strong binding. The top-performing compounds for INOSOX were predominantly flavonoids, including fisetin, pelargonidin, and luteolin, all exhibiting binding energies below -7.5 kcal/mol. These findings suggest that the identified compounds, particularly the flavonoids, have a strong propensity to interact with and potentially modulate INOSOX activity, highlighting their therapeutic relevance in inflammatory pathways.

Beyond the primary flavonoid cluster, chlorogenic acid and isoliquiritigenin also showed robust interactions with the human INOSOX protein (Herowati & Widodo, 2017), with binding energies significantly lower than those of the fatty acid derivatives and organic acids later in the docking hierarchy. Genistin and 9-HpODE follow closely, with the latter as the highest-ranking hydroperoxide derivative at -6.82 kcal/mol (Kim et al., 2024). Further down the ranking, nitrogen-containing compounds and other

organic acids, including trans-3-Indoleacrylic acid and 3,4-dihydroxyphenylacetic acid, show moderate binding affinities, whereas berberine shows a notably lower affinity for the INOSOX protein than for the IL-1 receptor (Liu et al., 2023). In contrast, 4-anisic acid and rutin occupy the intermediate range of the INOSOX docking profile, with rutin showing a binding energy of -6.02 kcal/mol, suggesting a less optimal fit than with the IL-1 receptor. Apocynin and L-phenylalanine further differentiate the two targets, with phenylalanine exhibiting a slightly improved binding energy of -6.50 kcal/mol when docked against INOSOX, as shown in Table 3.

Table 3 Molecular Docking Results for PDB ID (3E7G)

No	Compound Name	Binding Energy (kcal/mol)	Inhibition Constant (μM)
1	Meloxicam	-8.14	1.07
2	Isorhamnetin	-8.13	1.09
3	Scutellarin	-8.06	1.24
4	Quercetin	-7.96	1.47
5	Fisetin	-7.92	1.56
6	Pelargonidin	-7.86	1.74
7	Luteolin	-7.69	2.32
8	Chlorogenic acid	-7.37	3.95
9	Isoliquiritigenin	-7.33	4.20
10	Genistin	-6.94	8.18
11	(±)9-HpODE	-6.82	10.03
12	trans-3-Indoleacrylic acid	-6.70	12.29
13	3,4-Dihydroxyphenylacetic acid	-6.59	14.81
14	L-Phenylalanine	-6.50	17.11
15	Berberine	-6.10	34.00
16	4-Anisic acid	-6.07	35.36
17	Rutin	-6.02	38.42
18	Apocynin	-5.94	44.30
19	2.3-Dihydroxybenzoic acid	-5.86	50.90
20	3.5-Dihydroxybenzoic acid	-5.81	54.79
21	(+/-)12(13)-DiHOME	-5.58	80.92
22	Salicylic acid	-5.50	92.63
23	(+/-)9,10-dihydroxy-12Z-octadecenoic acid	-5.43	105.48
24	D-(-)-Quinic acid	-5.40	109.58
25	Vanillic acid	-5.40	110.89
26	Gallic acid	-5.35	119.93
27	Hexanoic acid	-5.30	129.31
28	Oleoyl ethanolamide	-5.18	159.59
29	8-Hydroxyquinoline	-5.10	182.84
30	Levulinic acid	-4.96	231.28
31	Proline	-4.91	251.21
32	Catechol	-4.65	392.29
33	Gluconic acid	-4.43	562.52
34	Methylsuccinic acid	-4.31	694.10
35	3-Hydroxybutyric acid	-4.24	781.50
36	2.5-Dihydroxybenzaldehyde	-4.10	992.81
37	D-(+)-Malic acid	-4.00	1.17
38	Succinic acid	-3.99	1.18
39	Betaine	-3.37	3.36
40	Choline	-3.00	6.32

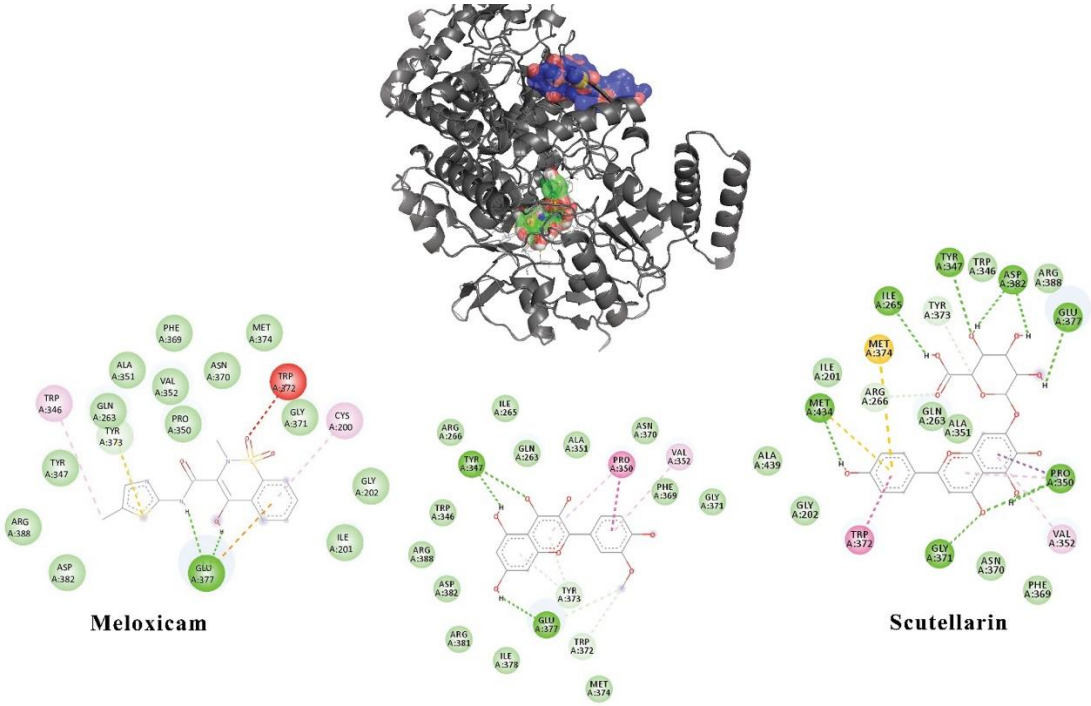

Figure 2 3D Visualization of the top three compounds, PDB ID 3E7G

Figure 2 presents the molecular docking results of three compounds: Meloxicam, Isohamnetin, and Scutellarin on the active site of a protein, probably the Cyclooxygenase-2 enzyme, as inferred from its amino acid residues. Meloxicam, a selective non-steroidal anti-inflammatory drug and COX-2 inhibitor, interacts with residues GLU 377 and TRP 372 via Pi-Sulfur bonding, which are crucial for stabilizing ligands in the COX-2 binding pocket. Isohamnetin, a flavonoid, displays a similar interaction profile, engaging GLU 377 and TYR 347, together with ARG 266 and ARG 388, suggesting strong binding affinity. Scutellarin shows a more intricate interaction network due to its glycoside structure, also binding GLU 377, ARG 388, and TYR 347, thereby occupying the same domain as Meloxicam and Isohamnetin. These findings align with prior studies identifying key residues like TYR 347 and ARG 106 for COX-2 inhibition, supporting the potential of Isohamnetin and Scutellarin as natural anti-inflammatory agents that block the COX-2 pathway at the molecular level.

Viability test

Figure 3 shows the viability of RAW 264.7 cells treated with 70% ethanol extract of *P. viridiflora* leaves at concentrations of 0.5, 5, 10, 15, and 25 µg/mL, as shown by the mean % of live cells. Increasing concentrations of the extract reduced RAW 264.7 cell viability. Extracts with cell viability over 90% indicated a non-toxic effect on RAW 264.7 cells, warranting further investigation.

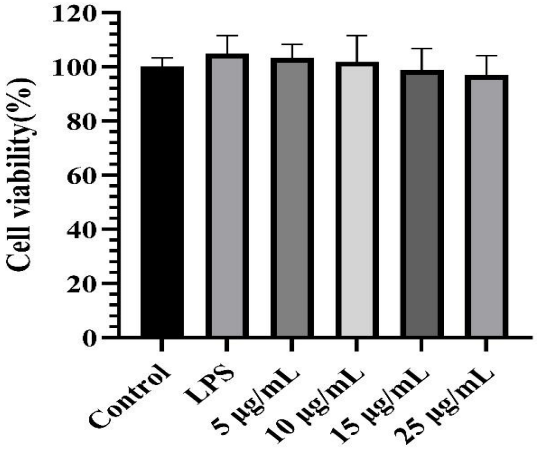

Figure 3. Cell viability of 70% ethanol extract of *P. viridiflora* leaves against RAW 264.7 at varying concentrations. The data are presented as mean ± SD (n=6). The X-axis represents the extract dose (µg/mL) and the control group (c). The Y-axis represents cell viability (%).

Nitric oxide

NO production was assessed by quantifying nitrite levels in the medium relative to untreated controls. RAW 264.7 cells stimulated with LPS exhibited elevated NO levels compared to the untreated control group (Fig. 4). A notable discrepancy in NO production was observed between the negative control group (LPS) and all other groups ($p<0.05$). Extracts at concentrations of 15 and 25 µg/mL demonstrated inhibition of NO production by as much as 81.2%.

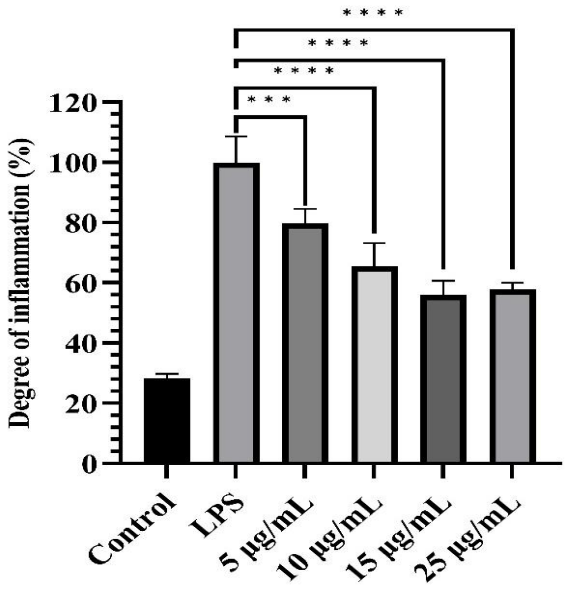

Figure 4. Effect of 70% ethanol extract of *P. viridiflora* leaf on NO production in RAW 264.7 cells. Data are presented as mean ± SD (n=4). X-axis: treatment groups (Control, LPS, and extract concentrations in µg/mL); Y-axis: degree of inflammation (%). Statistical significance: *** ($p < 0.001$) and **** ($p < 0.0001$) compared to the LPS group.

In RAW 264.7 cells, the NO level is a key marker of inflammatory activity. Although NO has vital physiological functions, such as immune defense against microorganisms, its overproduction has been linked to several illnesses, including atherosclerosis, diabetes, septic shock, autoimmune disorders, and chronic inflammatory diseases (Akanji et al., 2020). iNOS is the main regulator of NO synthesis, but excessive and prolonged NO production can cause inflammation-related tissue damage. LPS induces macrophage cells to secrete NO, leading to persistent inflammation. For example, when RAW 264.7 cells are stimulated to become inflamed, pro-inflammatory cytokines, including TNF-α and IL-6, rise significantly, and excessive NO generation increases to extremely high levels for 24 hours (Rahmawati et al., 2024).

Inflammatory vasodilation is linked to the protein iNOS, which is essential for NO synthesis. Excessive NO production, which has been connected to several disorders, can result from elevated iNOS levels. One possible treatment approach for inflammation and disorders marked by excessive NO production is iNOS inhibition (Herowati & Widodo, 2017; Kim et al., 2024). The anti-inflammatory potential of the 70% ethanol extract of *P. viridiflora* leaves was investigated by assessing its effect on nitric oxide production in LPS-stimulated RAW 264.7 cells, as shown in Figure 4. The extract inhibited NO generation in a concentration-dependent manner, significantly reducing NO levels compared with the LPS-stimulated control (100% inflammation) across all tested concentrations. 5 µg/mL reduced inflammation to 80% (20% inhibition) and 10 µg/mL to 65%, while higher doses of 15 and 25 µg/mL achieved the strongest effects (19% persistent inflammation, or 81% inhibition). Statistical analysis confirmed significant differences between all extract-treated groups and the LPS control.

This potent suppression of nitric oxide suggests that the leaf extract may mitigate cellular damage associated with DNA fragmentation and lipid peroxidation, which typically occur when reactive NO species react with oxygen (Thampithak et al., 2024). In particular, the expression of the iNOS gene in activated macrophages leads to the release of high concentrations of nitrite into the surrounding medium, which can be quantified using the Griess reagent assay to measure the degree of oxidative stress and inflammatory response (Negara & Choi, 2022; Yuste et al., 2015; Ahmad et al., 2020). This suppression is critical because overexpressed iNOS converts arginine into excessive NO, which can rapidly react with superoxide anions to form peroxynitrite, a highly potent oxidant that diffuses across phospholipid membranes and triggers further systemic inflammatory cascades (Xian et al., 2022).

Rat models of osteoarthritis induced by MIA

In MIA-induced OA rat models, disease progression was monitored for three weeks. This evaluation included rat joint diameter measurement (physical assessment), assessment of movement response to temperature stimuli using the hot plate method (functional evaluation), and quantification of pro-inflammatory cytokine IL-1β levels (biochemical analysis). Measuring joint diameter with a vernier caliper served as a physical parameter to confirm establishment of the OA model. Results showed that the MIA-induced group had significantly larger joint diameters (18.16 ± 0.17 mm) than the healthy, non-

MIA group (11.85 ± 0.34 mm; $p < 0.05$), as shown in Fig. 5, indicating successful establishment of the OA model in rats.

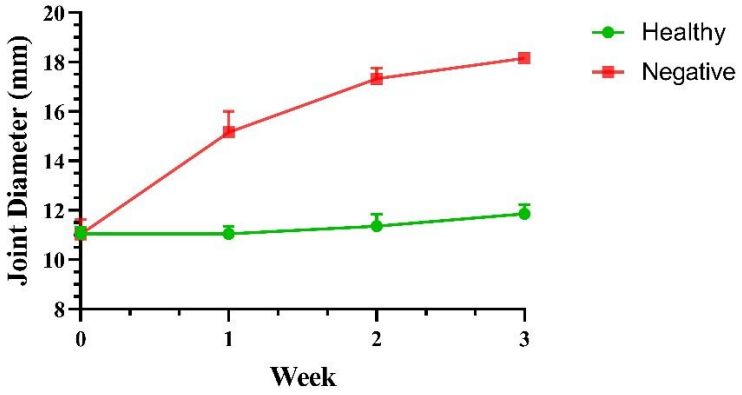

Figure 5. Joint diameters in rats during the development of an OA model with and without intra-articular induction of MIA. The data are presented as mean ± SD (n=5). The X-axis represents observation time (weeks), and the Y-axis represents the rat joint diameter (mm).

Rat functional characteristics or behavioral alterations in an inflammatory state can be used to assess the behavior of OA by assessing resistance (hyperalgesia) to responses to thermal stimulation of the hot plate method (Fig. 6). The results indicated that, with a significant difference ($p < 0.05$), the group subjected to MIA induction had a shorter hyperalgesia time in thermal stimulation (3.28 ± 0.44 s) than the healthy group (5.06 ± 0.34 s).

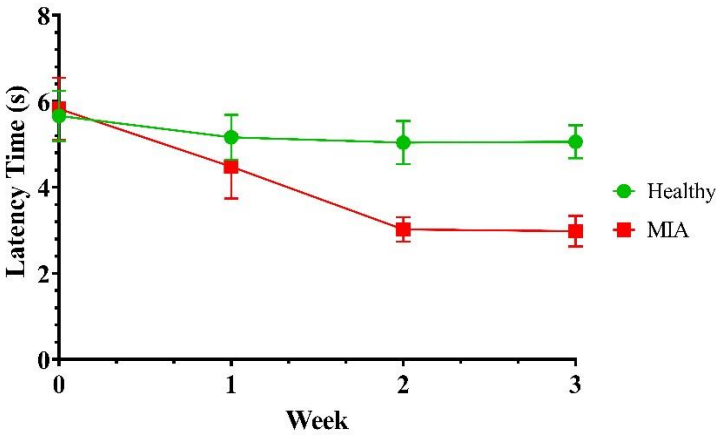

Figure 6. Hyperalgesia in rats during the development of an OA model with and without intra-articular induction of MIA. The data are presented as mean ± SD (n=5). The X-axis represents observation time (weeks), and the Y-axis represents latency time (seconds).

Before the rats received *P. viridiflora* extract, blood samples were collected three weeks after MIA injection to measure pro-inflammatory cytokine IL-1β levels using ELISA. This showed a significant difference ($p<0.05$) in IL-1β levels in the rats' blood serum. IL-1β levels in the MIA-induced group were roughly four times higher (2122.47 ± 101.53 pg/mL) than in the control group (482.33 ± 143. 38 pg/mL) (Fig. 7).

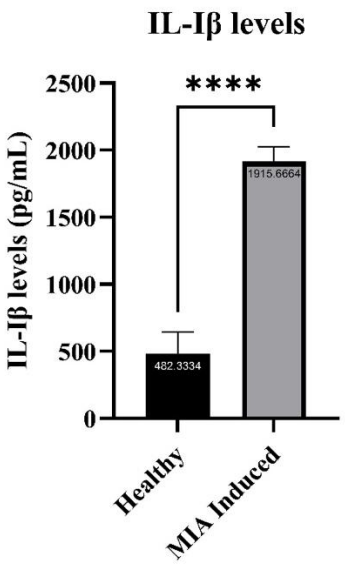

Figure 7. Levels of pro-inflammatory IL-Iβ cytokines in rat blood serum during the development of an OA model with and without intra-articular induction of MIA.

This in vivo experiment was performed in MIA-induced OA rat models to evaluate the extract's effects on IL-1β levels in a more complex biological setting. MIA, a glyceraldehyde-3-phosphate dehydrogenase inhibitor that reduces glycolysis, causes OA-like changes in articular cartilage by inhibiting the integration of chondral structures, resulting in chondrocyte death (Bao et al., 2022). Inhibition of glyceraldehyde-3-phosphate dehydrogenase leads to reactive oxygen species production. It increases COX-2, myeloperoxidase, and IL-1β. MIA causes acute inflammation associated with the expression of pro-inflammatory cytokines such as IL-1β, IL-5, IL-6, iNOS, COX-2, and MMP (Vincent, 2019; Moilanen et al., 2015). In addition to damaging articular cartilage, MIA causes inflammatory cell proliferation and increased pain (Khotib et al., 2020).

Effect of *Psychotria viridiflora* Reinw. Ex Blume leaves in OA rats

The physical parameters of knee diameter and heat-resistance time (hyperalgesia) were also measured at weeks 4, 5, 6, and 7 (post-extract administration). Furthermore, IL-1β concentration was quantified in serum samples during week 7. Results showed differences in knee diameter among the negative, positive, and treatment groups. The average diameter of the right knee joint during treatment indicated that several groups experienced a significant reduction in swelling. Joint swelling diameter decreased in the positive control group (meloxicam suspension). Three other groups, namely rats treated with a suspension of 70% ethanol extract of *P. viridiflora* leaves at doses of 5, 10, and 20 mg/200 g BW, also showed a reduction in the diameter of the right knee joint. The negative control group, which did not receive extract therapy, did not show a reduction in joint swelling diameter compared with the other four groups (Fig. 8).

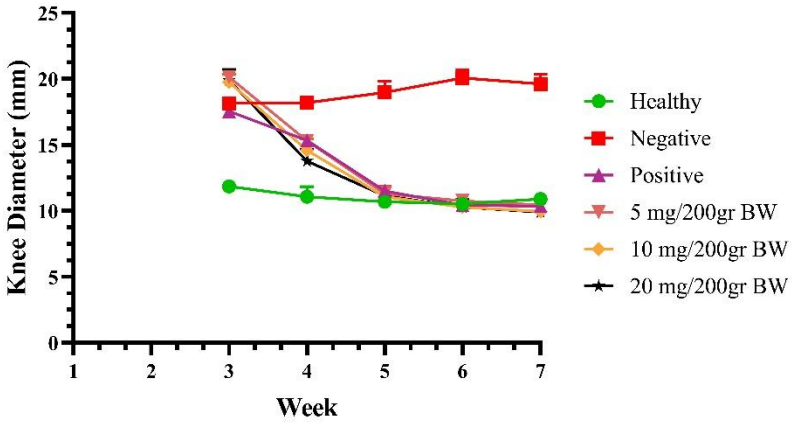

Figure 8. Joint diameter of rats in the OA rat model during treatment with dose variations of 70% ethanol extract of *P. viridiflora* leaves. The data are presented as mean ± SD (n = 5). The X-axis represents the observation time (weeks), and the Y-axis represents the diameter of the rat's joint in millimeters.

The results indicate that as the extract dosage increased, so did the latency time. The group receiving three doses of the extract showed no significant difference in heat retention time compared with the positive control group, which had an average retention time of six seconds. This suggests that the three doses of the extract can enhance heat retention time, a phenomenon known as hyperalgesia, as shown in Fig. 9.

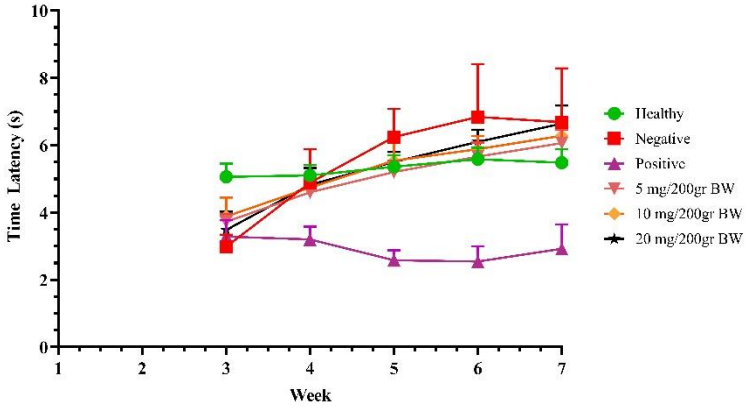

Figure 9. Latency time of rats in the OA rat model during treatment with dose variations of 70% ethanol extract of *P. viridiflora* leaves. The data are presented as mean ± SD (n=5). The X-axis represents observation time (week), and the Y-axis represents latency time (seconds).

These levels were compared to those measured during the third week (pre-test). The results showed that rats receiving extracts at doses of 5, 10, and 20 mg/200 g BW had significantly lower IL-1β levels in their blood serum, with mean reductions of 761.33, 631.33, and 594.67 pg/mL, respectively. These contrasted with the mean level of 1957.33 pg/mL in the negative control group (Fig. 10), suggesting that by reducing IL-1β levels, the three extract doses can successfully reduce knee swelling in rats.

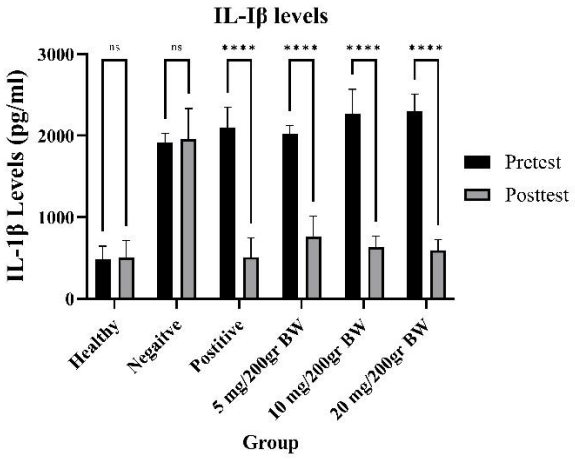

Figure 10. Levels of pro-inflammatory IL-Iβ cytokines in rat blood serum before and after treatment with dose variations from 70% ethanol extract of *P. viridiflora* leaves. The data are presented as mean ± SD (n=5). The X-axis represents the treatment group, and the Y-axis represents IL-1β pro-inflammatory cytokine levels (pg/mL) (*p<0.01).

Figure 10 presents the Interleukin-1 Beta (IL-1β) levels, quantified in picograms per milliliter (pg/ml), across various experimental groups, comparing Pretest and Posttest measurements. The "Healthy" control group maintained consistently low IL-1β levels, with a Pretest average of 482.3334 pg/ml and a Posttest average of 507.3334 pg/ml, showing no statistically significant difference between these time points. This establishes a stable, non-inflamed baseline. Conversely, the Negative control group, representing the disease model without intervention, exhibited persistently high IL-1β levels, with a Pretest average of 1915.666 pg/ml and a Posttest average of 1957.333 pg/ml, confirming a sustained inflammatory state. In the "Positive" control group and at all concentrations of the *P. viridiflora* extract, IL-1β levels increased significantly from their respective Pretest values, indicating successful inflammation induction.

The Positive control group, which served as a benchmark for anti-inflammatory efficacy, demonstrated a substantial reduction in IL-1β levels. Pretest levels were markedly high, averaging 2102.333 pg/ml, which were significantly attenuated to an average of 508.6668 pg/ml at Posttest ($p < 0.0001$). Similarly, the lowest administered concentration of the *P. viridiflora* extract, 5 mg/200gr BW, also exhibited a potent anti-inflammatory effect. Starting from high Pretest IL-1β levels, averaging 2023.667 pg/ml, the extract significantly reduced these levels to an average of 761.3334 pg/ml at Posttest ($p < 0.0001$), indicating a considerable mitigation of inflammation.

Increasing the extract dosage to 10 mg/200gr BW resulted in comparable efficacy. Pretest IL-1β levels, averaging 2270.333 pg/ml, were significantly lowered to an average of 631.3334 pg/ml at Posttest ($p < 0.0001$). The highest concentration tested, 20 mg/200gr BW, similarly showed a robust anti-inflammatory response, reducing Pretest IL-1β levels from an average of 2300.333 pg/ml to 594.6668 pg/ml at Posttest ($p < 0.0001$). Collectively, these findings indicate that all tested concentrations of the *P. viridiflora* extract effectively reduced IL-1β levels from their induced inflammatory state to values

comparable to the healthy baseline. While all three concentrations showed strong anti-inflammatory effects, a clear dose-dependent increase in efficacy was not distinctly observed among the Posttest values within this tested range.

P. viridiflora is used by inhabitants of West Kalimantan to relieve pain and inflammation in broken bones, with leaves being applied to the part of the body where the broken bone is located (Khotib et al., 2020). The 70% ethanol extract of this plant contains a variety of secondary metabolites, including alkaloids, saponins, flavonoids, and terpenoids. Based on LC-MS/MS QTOF analysis, this extract contains epicatechin, quercetin, isoorientin, kaempferol, [(5,7-dimethoxy-1H-indol-3-yl) methyl] dimethylamine, psychotridine, and p-coumaroylagmatine. The alkaloid group contains a monoterpene indolic alkaloid (N-β-glucopyranosyl vincosamide), which has been found to exhibit anti-inflammatory and analgesic properties by inhibiting the production of inflammatory mediators such as NO, IL-1β, and TNF-α.

Another alkaloid in this extract is psychotridine, which inhibits a crucial step in prostaglandin biosynthesis, specifically in the cyclooxygenase pathway, potentially reducing pain (Both et al., 2012). Furthermore, previous research has demonstrated that administering extracts from the stems and fruit of *P. nilgiriensis* at doses of 200 and 400 mg/kg BW induced substantial analgesic activity in rat models (Iniyavan et al., 2012).

OA development in the rat model typically occurred two to eight weeks after MIA administration at 1–4 mg/kg BW (Yamada et al., 2019). This rat model closely mimics OA progression in humans, providing a relevant and reliable platform for studying the disease and evaluating potential treatments. At a dose of 4 mg/kg BW in rats, OA histologically develops over 21 days. Rat knee diameter, time latency, and levels of the pro-inflammatory cytokine IL-1β are all observable. MIA increases capillary extravasation, cellular migration, and vascular permeability, which, in turn, triggers an inflammatory response. Knee swelling indicates synovial inflammation, a condition characteristic of the onset of osteoarthritis. The swelling restricted the rats' joint mobility and lasted several days.

In rat models of MIA-induced OA, the 70% ethanol extract of *P. viridiflora* leaves showed encouraging therapeutic benefits. Numerous indicators, such as decreased knee diameter, increased heat retention time, and reduced IL-1β levels, supported these findings. IL-1β is an important inflammatory cytokine associated with OA progression. The extract has strong anti-OA potential because of the strong link between IL-1β and NO in regulating MMP and ADAMTS.

CONCLUSIONS

In vitro research showed that the 70% ethanol extract of *P. viridiflora* efficiently suppresses NO generation in LPS-stimulated RAW 264.7 macrophage cells at different doses. Furthermore, in vivo tests in rat models of MIA-induced OA showed that this extract reduced IL-1β levels and knee width while extending heat retention duration. Two key chemicals involved in OA pathophysiology are NO and IL-1β. These results point to the extract's potential as an effective therapy for managing OA.

AUTHORS DECLARATIONS:

Ethics approval and consent to participate

The Animal Ethics Committee of the Faculty of Veterinary Medicine, Universitas Airlangga, Surabaya, Indonesia, approved the entire procedure through Ethical Clearance No. 2.KEH.118.07.2025. All methods were carried out in accordance with relevant guidelines and regulations, and the study is reported in accordance with the ARRIVE guidelines (https://arriveguidelines.org).

Patient consent for publication

Not applicable

Author contribution

RW: conceptualization, supervision, writing-review & editing; IS: formal analysis, writing-original draft; QAPP: investigation, data curation, formal analysis; DA: investigation, data curation, formal analysis; ADM: investigation, data curation, formal analysis; SSA: investigation, data curation, formal analysis; MODS: investigation, data curation, formal analysis; RRP: investigation, & data curation; SS: writing-review & editing, supervision; YW: writing-review & editing; MA: writing-review & editing; HC: supervision, validation, writing-review & editing.

Declarations of interest

The authors declare that they have no known competing financial interests or personal relationships that could have appeared to influence the work reported in this paper.

Data Availability

No data were used for the research described in the article.

Funding

The International Research Consortium of Universitas Airlangga provided funding for this study (No. 167/UN.3.LPPM/PT.01.03/2024).

Acknowledgments

The author appreciates the support and encouragement given by the university president and the head of the Institute for Research and Community Service, Universitas Airlangga, for the opportunity to obtain research funding under the International Research Consortium scheme (IRCON). Apart from that, the dean of the Faculty of Pharmacy, Universitas Airlangga, is thanked for supporting research facilities.

REFERENCES

Ahmad N, Ansari MY, Haqqi TM. Role of iNOS in osteoarthritis: pathological and therapeutic aspects. J. Cell Physiol 2020;235:6366-6376. https://doi.org/10.1002/jcp.29607

Akanji MA, Adeyanju AA, Rotimi D, Adeyemı OS. Nitric oxide balance in health and diseases: Implications for new treatment strategies. The Open Biochemistry Journal. 2020;14(1):25. https://doi.org/10.2174/1874091x02014010025

Arden N, Francisco JB, Bruyère O, Cooper C, Guermazi A, Hayashi D, Hunter D, Javaid KM, Rannou F, Roemer F, Reginster JY. Atlas of Osteoarthritis. *Second ed. Springer Healthcare Ltd*, London; 2012.

Bao Z, Chen M, Li C, Shan Q, Wang Y, Yang W. Monosodium iodoacetate-induced subchondral bone microstructure and inflammatory changes in an animal model of osteoarthritis. Open Life Sciences 2022;17(1):781-793. https://doi.org/10.1515/biol-2022-0079

Berger A, Preinfalk A, Robien W, Brecker L, Valant-Vetschera KM, Schinnerl J. New reports on flavonoids, benzoic- and chlorogenic acids as rare features in the *Psychotria alliance* (Rubiaceae). Biochemical Systematics and Ecology. 2016;66:145. https://doi.org/10.1016/j.bse.2016.02.027

Bo SX, Jie WY, Chao CD, Sai M, Zhe W, Kun ZY, Hui GH, Chen W, Xiao M, Yao HZ, Ran YH, Sen ZJ, Dan CW. An inducible nitric oxide synthase dimerization inhibitor prevents the progression of osteoarthritis. Front Pharmacol. 2022;13:861183. https://doi.org/10.3389/fphar.2022.861183

Both FL, Kerber VA, Henriques AT, Elisabetsky E. Analgesic properties of Umbellatine from *Psychotria umbellata*. Pharm. Biol. 2012;40:336-341. https://doi.org/10.1076/phbi.40.5.336.8453

Chen Q, Toy JYH, Seta C, Yeo TC, Huang D. Inhibition effect of extract of *Psychotria viridiflora* stem on α-amylase and α-glucosidase and its application in lowering the digestibility of noodles. Frontiers in Nutrition. 2021;8:701114. https://doi.org/10.3389/fnut.2021.701114

Doğan HO. Review of metabolomics: A review of liquid chromatography mass spectrometry-based methods and clinical applications. Turkish Journal of Biochemistry 2024;49(1):1. https://doi.org/10.1515/tjb-2023-0095

Eitner A, Müller S, König C, Wilharm A, Raab R, Hofmann GO, Kamradt T, Schaible HG. Inhibition of inducible nitric oxide synthase prevents IL-1β-induced mitochondrial dysfunction in human chondrocytes. Int. J. Mol. Sci 2021;22: 2477. https://doi.org/10.3390/ijms22052477

Formagio ASN, Volobuff CRF, Kassuya CAL, Cardoso CAL, Carmo Vieira MD, Pereira ZV, Bagatin MC, de Freitas Gauze G. *Psychotria leiocarpa* extract and vincosamide reduce chemically induced inflammation in mice and inhibit acetylcholinesterase activity. Inflammation 2019;42:1007-1018. https://doi.org/10.1007/s10753-019-01018-w

Goldring MB, Otero M. Inflammation in osteoarthritis. Curr. Opin. Rheumatol. 2011;23:471-478. https://doi.org/10.1097/bor.0b013e328349c2b1

Heijink A, Gomoll AH, Madry H, Drobnič M, Filardo G, Sprogueira-Mendes J, Van Dijk CN. Biomechanical considerations in the pathogenesis of osteoarthritis of the knee. Knee Surg. Sport. Traumatol Arthrosc. 2012;20:423-435. https://doi.org/10.1007/s00167-011-1818-0

Henao-Murillo L, Pastrama M, Ito K, Donkelaar CC. The relationship between proteoglycan loss, overloading-induced collagen damage, and cyclic loading in articular cartilage. Cartilage. 2021;13(2):501S1-1512S. https://doi:10.1177/1947603519885005

Herowati R, Widodo GP. Molecular Docking Analysis: Interaction Studies of Natural Compounds to Anti-inflammatory Targets. InTech eBooks.2017. https://doi.org/10.5772/intechopen.68666

644 Iniyavan M, Sangeetha D, Saravanan S, Parimelazhagan T. Evaluation of antioxidant and
645 pharmacological properties of *Psychotria nilgiriensis* Deb & gang. Food Sci. Biotechnol.
646 2012;21:1421-1431. https://doi.org/10.1007/s10068-012-0187-x

647 Kachlicki P, Piasecka A, Stobiecki M, Marczak Ł. Structural characterization of flavonoid
648 glycoconjugates and their derivatives with mass spectrometric techniques. Molecules
649 2016;21(11):1494. https://doi.org/10.3390/molecules21111494

650 Khotib J, Pratiwi AP, Ardianto C, Rahmadi M. Attenuation of IL-1β on the use of glucosamine as an
651 adjuvant in meloxicam treatment in rat models with osteoarthritis. J. Basic Clin. Physiol.
652 Pharmacol. 2020;30:0332. https://doi.org/10.1515/jbcpp-2019-0332

653 Kim HH, Jeong SH, Park MY, Bhosale PB, Abusaliya A, Lee SJ, Heo JD, Kim H, Seong JK, Kim D,
654 Park K, Kim GS. Binding affinity screening of polyphenolic compounds in *Stachys affinis* extract
655 (SAE) for their potential antioxidant and anti-inflammatory effects. Research Square. 2024.
656 https://doi.org/10.21203/rs.3.rs-4089363/v1

657 Kolasinski SL, Neogi T, Hochberg MC, Oatis C, Guyatt G, Block J, Callahan L, Copenhaver C, Dodge
658 C, Felson D, Gellar K, Harvey WF, Hawker G, Herzig E, Kwoh CK, Nelson AE, Samuels J,
659 Scanzello C, White D, Wise B, Altman RD, DiRenzo D, Fontanarosa J, Giradi G, Ishimori M,
660 Misra D, Shah AA, Shmagel AK, Thoma LM, Turgunbaev M, Turner AS, Reston J. American
661 College of Rheumatology/Arthritis Foundation Guideline for the Management of Osteoarthritis of
662 the Hand, Hip, and Knee. Arthritis Care Res 2019;72:149-162. https://doi.org/10.1002/acr.24131

663 Leong D, Choudhury M, Hirsh D, Hardin J, Cobelli N, Sun H. Nutraceuticals: potential for
664 chondroprotection and molecular targeting of osteoarthritis. Int. J. Mol. Sci. 2013;14:23063-23085.
665 https://doi.org/10.3390/ijms141123063

666 Leonidou A, Lepetsos P, Mintzas M, Kenanidis E, Macheras G, Tzetis M, Potoupnis M, Tsiridis E.
667 Inducible nitric oxide synthase as a target for osteoarthritis treatment. Expert Opin. Ther. Targets
668 2018;22:299-318. https://doi.org/10.1080/14728222.2018.1448062

669 Liu T, Chen YK, Adil M, Almehmadi M, Alshabrmi FM, Allahyani M, Alsaiari AA, Liu P, Khan MR,
670 Peng Q. In silico identification of natural product-based inhibitors targeting the IL-1β/IL-1R
671 protein–protein interface. Molecules 2023;28(13):4885.
672 https://doi.org/10.3390/molecules28134885

673 Matsuura HN, Porto DD, Fett-Neto AG. Bioactive alkaloids from South American Psychotria and related
674 Rubiaceae. Natural Products 2013;119-147.

675 Moilanen LJ, Nummenmaa E, Hamalainen M. Monosodium iodoacetate-induced inflammation and joint
676 pain are reduced in TRPA1-deficient mice: potential role of TRPA1 in osteoarthritis. Osteoarthritis
677 Cartilage. 2015;23(1):2017-2026. https://doi.org/10.1016/j.joca.2015.09.008

678 Nagy E, Vajda E, Vari C, Sipka S, Fárr AM, Horváth E. Meloxicam ameliorates the cartilage and
679 subchondral bone deterioration in monoiodoacetate-induced rat osteoarthritis. Peer 2017;5:e3185.
680 https://doi.org/10.7717/peerj.3185

681 Negara B, Choi JS: *Bifidobacterium lactis* inhibits iNOS expression in LPS-stimulated RAW 264.7
682 macrophages. Indonesia. Biomed J. 2022;14(2022):199-205.
683 https://doi.org/10.18585/inabj.v14i2.1929

684 Queiroz GS, Luz ABG, Nascimento MVPDS, Thomasi SS, Ferreira AG, Dalmarco EM, Brighente IM C.
685 Phytochemical study and anti-inflammatory effect of *Psychotria stenocalyx* (Rubiaceae). Journal
686 of Applied Pharmaceutical Science. 2017;7(4), 168–173.
687 https://doi.org/10.7324/JAPS.2017.70425.

688 Rahmawati SI, Indriani DW, Ningsih FN, Hardhiyuna M, Firdayani F, Ahmadi P, Rosyidah A, Septiana
689 E, Dharmayanti NLPI, Bayu A, Putra MY. Dual anti-inflammatory activities of COX-2/5-LOX

driven by kratom alkaloid extracts in lipopolysaccharide-induced RAW 264.7 cells. Research Square.2024. https://doi.org/10.21203/rs.3.rs-4628929/v1

Rajapakse N, Kim MM, Mendis E, Kim SK. Inhibition of inducible nitric oxide synthase and cyclooxygenase-2 in lipopolysaccharide-stimulated RAW 264.7 cells by carboxybutyrylated glucosamine takes place via down-regulation of mitogen-activated protein kinase-mediated nuclear factor-kappa B signal. Immunology. 2018;123:348-357. https://doi.org/10.1111/j.1365-2567.2007.02683.x

Sari RA, Luthfiana F, Sholihah I, Matsunami K, Widyowati R. Antiosteoarthritis activities of 70% ethanol extract of *Eleutherine bulbosa* (Mill.) Urb. bulb on rats with monosodium iodoacetate-induced osteoarthritis. J. Public Health Africa 2023;14:2506. https://doi.org/10.4081/jphia.2023.2506

Smith HS, Baird W. Meloxicam and selective COX-2 inhibitors in the management of pain in the palliative care population. Am. J. Hosp. Palliat. Care. 2023;20:297-306. https://doi.org/10.1177/104990910302000413

Solomon DH, Husni ME, Wolski KE, Wisniewski LM, Borer JS, Graham DY. The precision trial investigators, differences in the safety of nonsteroidal anti-inflammatory drugs in patients with osteoarthritis and patients with rheumatoid arthritis. Arthritis & Rheumatol 2011;70(4): 537-546.

Thampithak A, Karachot B, Jantaratnotai N, Tuchinda P, Sanvarinda P. Anti-inflammatory effects of *Moringa oleifera* Lam leaf extract in lipopolysaccharide-activated microglia. Trends in Sciences. 2024;21(5):7407. https://doi.org/10.48048/tis.2024.7407

Vincent TL. IL-1 in osteoarthritis: time for a critical review of the literature. Research 8:F1000-Faculty, 2019. https://doi.org/10.12688/f1000research.18831.1

Widyowati R, Haryadi D, Chang HI, Suryawan IPG, Utama A. The effect of *Rusa unicolor* antler extracts from East Kalimantan in bone turnover cell models. Turkish J. Pharm. Sci. 2019;17:440-445. https://doi.org/10.4274%2Ftjps.galenos.2019.57805

Widyowati R, Purwitasari N, Oktarina RD, Ekasari W, Khairunnisa S, Chang HI. Exploration of several plants from Baung Forest on bone formation cell models. J. Basic Clin. Physiol. Pharmacol. 2021;32:831-837. https://doi.org/10.1515/jbcpp-2020-0489

Widyowati R, Suciati S, Hariyadi DM, Chang HI, Suryawan IPG, Tarigan N, Sholikhah I, Ardianto C, Nurhan AD, Sagitaras IB. The pro-inflammatory cytokine Il-Iβ alteration by deer (*Rusa Unicolor*) antler extract on osteoarthritis rat model. Saudi Pharmaceutical Journal 2023;31(6):1109-1114. https://doi.org/10.1016/j.jsps.2023.03.022

Yamada EF, Salgueiro AF, da A, Goulart S, Mendes VP, Anjos BL, Folmer V, da Silva MD. Evaluation of monosodium iodoacetate dosage to induce knee osteoarthritis: Relation with oxidative stress and pain. Int. J. Rheum. Dis. 2019;22:399-410. https://doi.org/10.1111/1756-185x.13450

Yan B, Wang D, Dong S, Cheng Z, Na L, Sang M, Yang H, Yang Z, Zhang S, Yan Z. Palmatine inhibits the TRIF-dependent NF-κB pathway against inflammation induced by LPS in goat endometrial epithelial cells. Int. Immunopharmacol. 2017;45:194-200. https://doi.org/10.1016/j.intimp.2017.02.004

Yang H, Zhang H, Yang C, Chen Y. Chemical constituents of plants from the Genus Psychotria. Chem. Biodivers 2016;13:807-820. https://doi.org/10.1002/cbdv.201500259

Yuste JE, Tarragon E, Campuzano CM, Ros-Bernal F. Implications of glial nitric oxide in neurodegenerative diseases. Front. Cell. Neurosci. 2015;9:322. https://doi.org/10.3389/fncel.2015.00322

Zhu L, Lin X, Li S, Sun D, Fang H, Xu J, Huang J, Li G. Effect and mechanism of applying *Myriophyllum verticillatum* for reclaimed water purification in urban rivers. Water 2023;15(13):2331. https://doi.org/10.3390/w15132331